Appl. Phys. B 85, 329–336 (2006)
DOI: 10.1007/s00340-006-2364-1

Applied Physics B
Lasers and Optics

A. RIDDLE✉
M. SELKER

Impedance-optimized photo-acoustic spectroscopy

Finesse, Inc., 3230 Scott Blvd, Santa Clara, CA 95054, USA

Received: 3 April 2006/Revised version: 18 May 2006
Published online: 10 August 2006 •

ABSTRACT We have examined the basic assumptions leading to optimized performance of small photo-acoustic resonators. Previous attempts at miniaturizing photo-acoustic systems have found the loading of the microphone on the cavity to be insignificant. We have shown theoretically and tested experimentally the fact that the microphone loading can have a dramatic effect on the resonator behavior. Treatment of the pressure and volume velocity of the sound waves as analogs of voltage and current facilitates the use of standard electrical engineering techniques and leads to techniques that enable one to efficiently optimize the impedance match between the cavity and the microphone.

PACS 43.35.Ud; 43.20.Ks; 43.20.Mv

1 Introduction

Discovery of the photo-acoustic effect and resonant acoustic enhancement of the photo-acoustic effect has been known for over 120 years [1, 2]. Despite the length of time that this effect has been known and understood the migration of this technique into mainstream technology, and in particular its adoption in mainstream gas detection, has been slow. The advent of infrared gas lasers in the 1970s and 1980s led to strong interest in optical spectroscopy and optical methods for sensitive gas detection – including the photo-acoustic effect and photo-acoustic-based detectors [3, 4]. Unfortunately the general size, inefficiency, and lack of portability of the gas lasers utilized in these systems generally confined their use to laboratory environments. The recent telecommunications boom provided a solution to the aforementioned issues with gas lasers by providing compact, efficient, and relatively inexpensive semiconductor lasers with wavelengths extending into the near infrared (NIR). This combined with renewed interest in environmental sensing and semiconductor manufacturing quality control requirements has stimulated research into ultra-sensitive, compact, spectroscopic-based sensors generally, and diode-laser-based photo-acoustic sensors in particular [5, 6].

While availability of NIR semiconductor lasers has solved some of the issues associated with making sensitive, compact gas detectors others still remain. The generally modest powers supplied by NIR semiconductor lasers are typically at wavelengths corresponding to overtone absorptions rather than the fundamentals. This typically leads to a situation where there is a reduced percentage of absorption of an already low power source. The resulting lower value for absorbed power in turn leads to lower sensitivities for semiconductor laser based spectroscopy systems. The desire to move to ever smaller footprints can also lead to design trade-offs that affect performance. Even casual investigation of these trade-offs leads to questions regarding the optimal photo-acoustic resonator design for a given source and footprint.

The generally accepted formalism for optimizing the sensitivity of a resonantly excited photo-acoustic system calls for placing the microphone in the center of the acoustic resonator, reducing the acoustic scattering losses, eliminating compliance in the cell walls, and generally minimizing cavity volume while optimizing the acoustic Q [7, 23]. As Q is defined as the ratio of the energy stored per cycle compared to the energy lost, some of these edicts seem at odds; the smaller the volume of the cavity the less energy the resonator can store and often the smaller the absorbed power. Irrespective of this fact, recent works have described efforts to move to smaller systems both for portability [5] as well as for applicability in ultra-sensitive detection of chemical composition in mesoscale analysis systems [8, 9]. Interestingly, none of the miniaturized systems have resulted in the enhanced performance predicted by first-order theory. We explore here some of the basic design issues related to maintaining sensitivity while miniaturizing semiconductor laser based photo-acoustic systems. It is shown that the microphone loading of the cavity must be taken into account in order to accurately predict the performance of the cell and thereby maximize performance. The analogy between fundamental analog electrical engineering and acoustics [7, 10] is extended to show how the position of the microphone in the cavity is a critical variable which can be used to optimize performance.

2 Theory

Designing small photo-acoustic cells involves several challenges. The cell sensitivity equation given in (1) was derived by Kreuzer for cylindrical cells [4]. This equation shows that increasing cell Q and decreasing cell vol-

✉ Fax: +1 408 327 6699, E-mail: ariddle@finesse-inc.com

ume should increase cell sensitivity without limit. Practically speaking, several limits exist to increasing the cell sensitivity. The first limit is that smaller cell diameters reduce the cell Q [4]. The second limit, apparently not commonly known, is that smaller cell diameters increase the acoustic impedance of the cell to the point that the impedance of commonly used electret microphones limits the cell Q. We will explore this second limitation in the following discussion by both analysis and measurements.

$$S_{\mathrm{PAS}} = \frac{(\gamma - 1)\, P\alpha l Q_{\mathrm{ac}}}{V\omega}\,, \tag{1}$$

$$S_{\mathrm{PAS}} = \frac{(\gamma - 1)\, P\alpha Q_{\mathrm{ac}}}{\omega\pi r^2}\,. \tag{2}$$

In the above equations S_{PAS} is the cell sensitivity, γ is the adiabatic gas constant, P is the optical power in watts, α is the absorption in cm^{-1}, l is the optical path length in cm, Q_{ac} is the acoustic Q of the cell, V is the volume of the cell, ω is 2π times the frequency in hertz, and r is the radius of the cell.

In (1), the physics of acoustics provides a link between cell Q and cell volume so that these terms cannot be independently optimized. For cylindrical cells the volume can be written as the product of cross-sectional area and length, so the length term in the numerator will cancel part of the volume term in the denominator. Equation (2) shows (1) with the cell length canceled. Equation (2) shows that reducing the cell radius, r, can increase the cell sensitivity as the inverse square of the radius. The cell Q is also dependent on the cell radius because the boundary layer of air along the cylinder wall is the primary loss in a closed, rigid, nonporous cell [10]. Using dimensional analysis shows that maximizing Q does not optimize cell sensitivity for a cylindrical cell, but that cell sensitivity is proportional to $\sqrt{l}/r$ [11]. Measurements of cylindrical tube Qs are shown in Fig. 1. These measurements were made by exciting tubes at one end and measuring the transmission out of the other end. Each tube was placed in a port of an acoustic isolation chamber with a loudspeaker as an acoustic source inside the isolation chamber. A microphone was placed at the opposite end of the tube just outside the isolation chamber to measure the transmission response. By measuring the transmission response of the tube the center frequency and half power points of the tube resonance could be measured. Because the Q of a resonator is defined as the resonant frequency divided by the half-power bandwidth, Q can be computed from the transmission measurement. Figure 1 shows a dramatic decrease in Q for radii below 1 mm. The simulation results in Fig. 1 include both the boundary layer loss and open end effects described in Sect. 5. A volumetric loss term also exists, but it is negligible in this situation.

$$Z_{\mathrm{o}} = \frac{\varrho c}{\pi r^2}\,. \tag{3}$$

The wave impedance of a cylindrical tube is given by (3), where ϱ is the density of air, c is the speed of sound, and r is the tube radius [10]. Tube acoustic wave impedance is plotted in Fig. 2 versus radius. A model of the acoustic impedance of a typical small electret microphone is given in Fig. 3. A plot of the acoustic impedance of a Knowles EK3133 is shown in Fig. 4. It may initially appear that the tube wave impedances shown in Fig. 2 are so much greater than the microphone impedance that there should be no concern until cell diameters are well below 1 mm. In reality, the effective loss resistance of a tube is Q times the wave impedance of the tube [12]. This loss resistance can be determined by multiplying the Q measurements of Fig. 1 with the wave impedance given in (3). Figure 5 shows impedances much greater than the microphone impedance shown in Fig. 4.

By comparing the impedances in Figs. 4a and 5 we can see that the microphone resistance is significantly smaller than the equivalent acoustic resistance of the tube, which causes the presence of a microphone to alter the total Q of the tube and affect the maximum pressure level in the tube. Equation (4) below describes the total Q of a tubular cell with a microphone loss R_{mic}, when the microphone is placed at the center of the resonator [12].

$$Q_{\mathrm{T}} = \frac{Q_{\mathrm{ac}} R_{\mathrm{mic}}}{Q_{\mathrm{ac}} Z_{\mathrm{o}} + R_{\mathrm{mic}}}\,. \tag{4}$$

In (4), Q_{T} is the total acoustic Q of the tube and microphone, Z_{o} is the impedance of the tube, Q_{ac} is the acoustic Q of the tube, and R_{mic} is the acoustic resistance of the microphone.

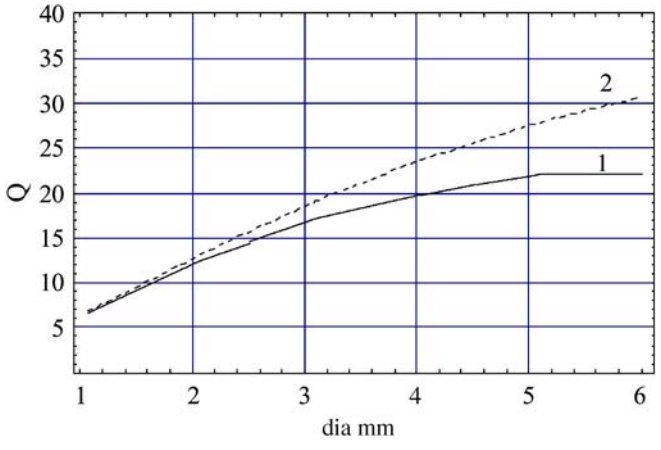

FIGURE 1 Measurements and simulations of Q versus diameter (mm) for tubes of approximately 1-, 2-, 3-, 4-, 5-, and 6-mm diameters and 100-mm length. *Line 1* are measurements and *line 2* are simulations

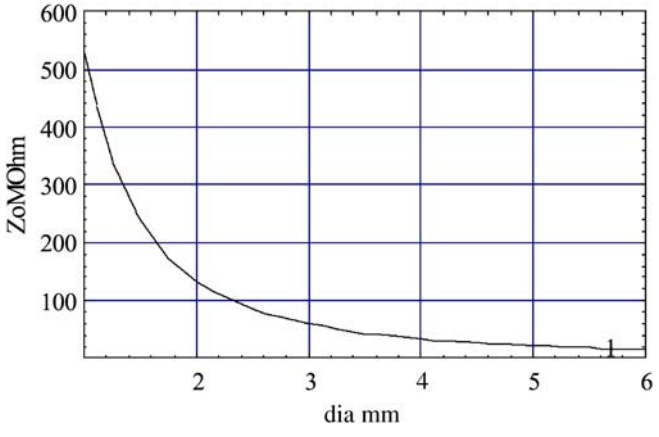

FIGURE 2 Plot of acoustic impedance versus tube diameter (mm). The tube impedance is given in acoustic megohms

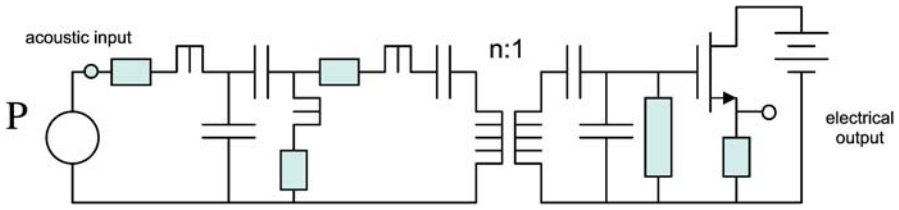

FIGURE 3 Knowles electret acoustic model for EK series. Values are available on the Knowles web site

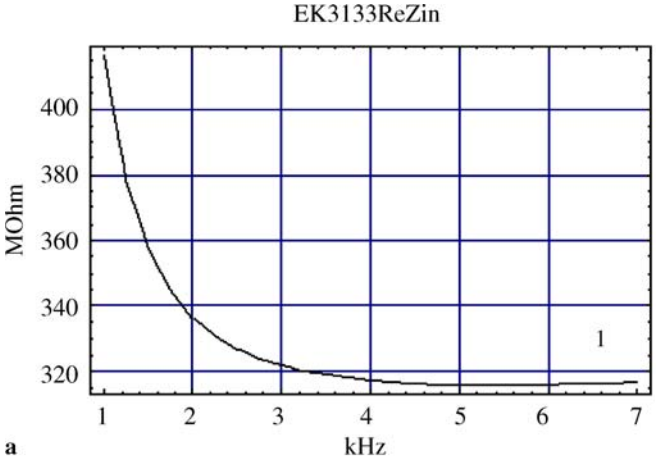

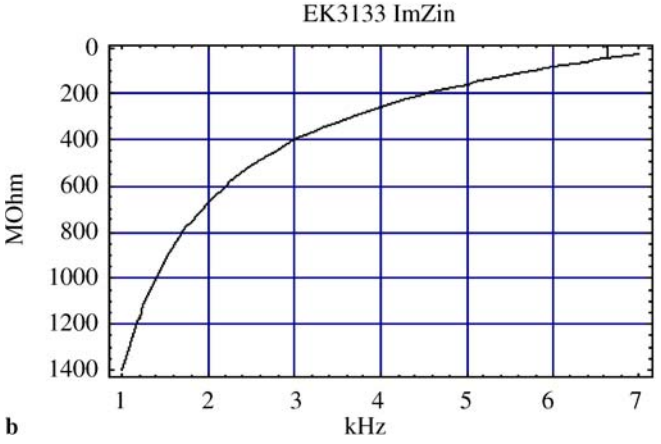

FIGURE 4 Plot of microphone impedance versus frequency: (**a**) real part of Zin; (**b**) imaginary part of Zin. The axes are in megohms and kilohertz

From this equation it can be seen that as the microphone resistance becomes very large the total Q is equal to the acoustic Q of the tube. As the microphone resistance becomes small compared to $Q_{ac}Z_o$ the total Q is reduced by the ratio of R_{mic} to $Q_{ac}Z_o$. A direct and simple solution to this problem would be to construct microphones with higher acoustic impedances. Unfortunately, microphones with these impedances, which are also physically suitable for mounting in small cylinders ($<$ 2.5-mm diameter), are not commercially available at the desired sensitivity. The Knowles EK3133 requires a mounting hole of approximately 2 mm, which makes it very useful for miniature photoacoustic spectroscopy (PAS) cells.

Given that it is difficult to find a microphone that solves the problem directly, we have developed another approach. This approach is to move the microphone off the center of the cell to change how much the microphone reduces the cell Q. This may seem counterintuitive at first, but can be easily explained. A plot of pressure variation along a cylindrical cell is

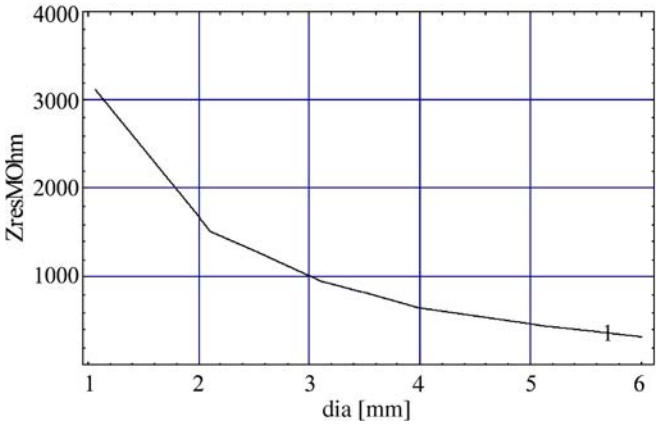

FIGURE 5 Plot of equivalent acoustic loss resistance at the center of a tube versus the tube diameter

shown in Fig. 6. This plot shows a pressure maximum at the center of the cell, where the microphone is typically placed to take advantage of the pressure maximum [4, 7, 8, 11, 13]. As the microphone is moved away from the center the available pressure is reduced according to (5) [10]. This fact is more than compensated for by the fact that the loading of the microphone on the cell is reduced by the square of (5). Using electrical analogs can show how this works, as it has been done for many years in antenna and filter design [12].

$$P = P_o \cos(\pi x/l)\,. \tag{5}$$

In (5), x varies from $-l/2$ to $l/2$, where l is the length of the cell and P_o is the maximum pressure. Equation (5) shows that the pressure has a maximum in the center and a minimum at each end of the cell, or tube in this example. The acoustic volume velocity has the opposite characteristic in that the vel-

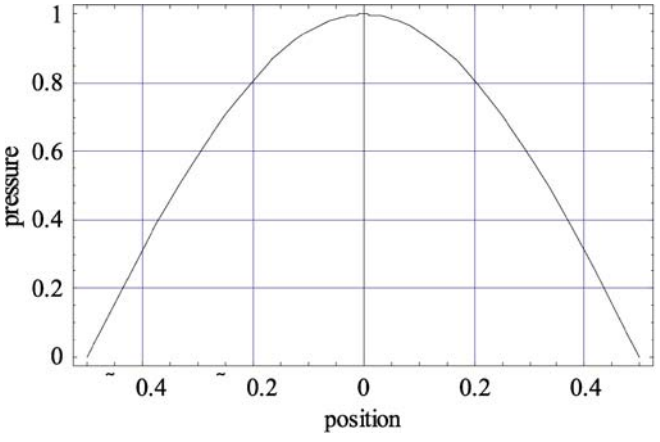

FIGURE 6 Plot of pressure variation along the length of a cylindrical tube with the tube extending from -0.5 to 0.5

ocity is at a maximum where the pressure is at a minimum and vice versa. Figure 6 shows the ratio of pressure to volume velocity at the center of a tube at the resonant frequency, because the acoustic impedance is the ratio of pressure to volume velocity [10]. As we move away from the center of the cell the volume velocity increases and the pressure reduces, so that at some point the ratio will equal that of the microphone resistance. At this point we have matched the cell impedance to the microphone resistance, and maximum power transfer between the cell and the microphone will occur at this point for a resistively dominated microphone [12, 22].

Impedance matching has several consequences familiar to electrical engineers; it allows a cell to have half its potential Q (Q without a microphone) and it allows the maximum signal to be delivered to the microphone. Moving the microphone off the center of the cell will change R_{mic} to $n^2 R_{\mathrm{mic}}$ in (4), where $n = 1/\cos(\pi x/l)$. This movement of the microphone off the cell midpoint increases the cell Q and increases the pressure at the center of the cell as n^2 if the losses are dominated by the microphone. As the microphone is moved off the center of the cell the center pressure increases as n^2 (until cell losses begin to dominate) while the pressure at the microphone is reduced according to $1/n$. Depending on the ratios of R_{mic} to the equivalent acoustic loss resistance of Fig. 5, the resulting pressure curve versus distance can range from Fig. 6 to some variation of Fig. 7.

3 System

In order to test the basic elements of the aforementioned theory, a simple test-bed was developed and implemented. The test-bed utilized brass tubes with open ends so that the air inside the tubes was moisture laden and with a content that could be readily calculated based on temperature and relative humidity. The photo-acoustic signal generated was based on excitation of the $(3, 0, 3) \leftarrow (2, 0, 2)$ rotational transition in the $\nu_1 + \nu_3$ vibrational band of H_2O [14].

The system as shown in Fig. 8 consisted of a 20-mW NEL distributed feedback (DFB) laser with a vacuum wavelength of 1392.5304 nm. The fiber-coupled laser beam was collimated and then focused through our open cells in order to eliminate the possibility of mode scraping leading to heating of the walls. The resulting Gaussian beam radius, ω, was less than 1/4.6 of the tube's diameter at its largest point [15]. The path between the optics and the entrance to the cell was minimized in order to avoid pre-distortion of the modulated pump beam by atmospheric absorption. The cells were all approximately 2 mm in diameter and 35 mm in length; however, in accordance with our theory the position of the microphone relative to the centerline of the cell was varied. The DFB temperature and current were controlled using an ILX Lightwave diode controller.

We employed wavelength-modulation spectroscopy (WMS) [16] and $2f$ detection [17] in order to resonantly excite our cell and enhance the sensitivity. As dictated by the theory, we adjusted the modulation depth of our laser to ~ 2.2 half widths at half maximum (HWHM). For completeness, we investigated the effect of the intensity modulation of the DFB laser on the overall $2f$ sensitivity peak using a recently published analytical technique [13]. The effect was found to be minimal as shown by the results of our simulation in Fig. 9. Given the chirp parameter of our laser, we found that in terms of optimal modulation depth there was very little departure

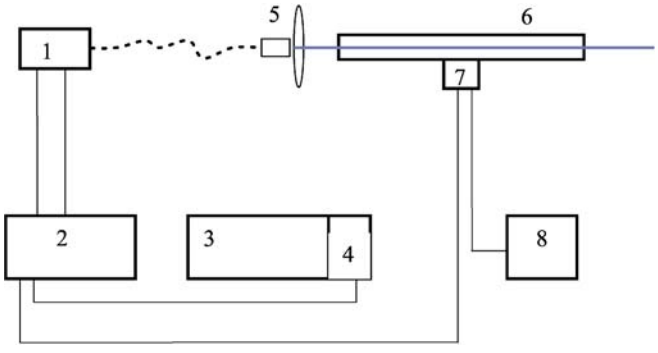

FIGURE 8 The experimental set-up. 1 is the NEL DFB, 2 is the diode controller, 3 is the lock-in amplifier, 4 is the frequency synthesizer, 5 is the optical train, 6 is the acoustic resonator, 7 is the microphone, and 8 is the power supply

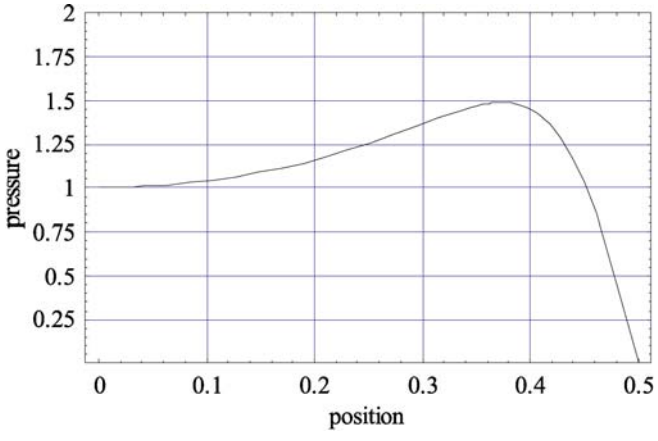

FIGURE 7 Microphone response versus microphone offset for an equivalent acoustic loss impedance of 200 MΩ and a microphone resistance of 300 MΩ, normalized to the response with the microphone at the center of the cell. The figure is the multiplication of $1/n$ with $Z_{\mathrm{eq}} n^2 R_{\mathrm{mic}}/(Z_{\mathrm{eq}} + n^2 R_{\mathrm{mic}})$, where Z_{eq} is the equivalent acoustic loss resistance shown in Fig. 5

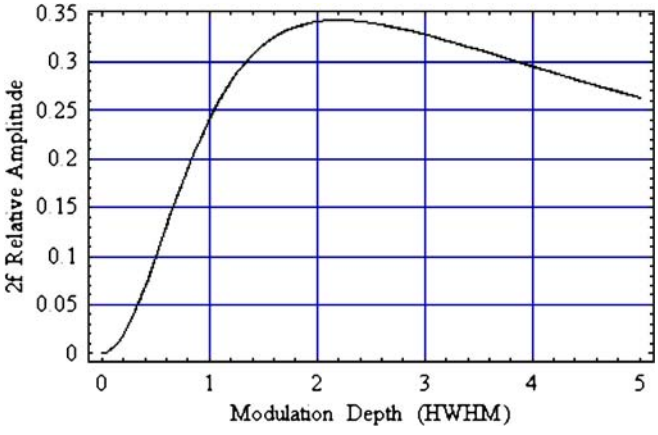

FIGURE 9 Plot of the amplitude of the $2f$ signal relative to the fundamental as a function of modulation depth in half widths at half maximum. The curves for pure frequency modulation (FM) and combined intensity modulation and frequency modulation (IM-FM) are lying on top of each other

of our intensity- and frequency-modulated laser from an ideal frequency-modulated laser.

The drive current to the laser was modulated in 10-Hz steps from 500 Hz to 3500 Hz using the frequency synthesizer on our SRS 830 lock-in amplifier to drive the laser diode controller. The acoustic signal was detected using a Knowles EK3133 electret microphone, and the electrical signal was detected using our lock-in amplifier. The entire data-acquisition process was automated using LabView®.

As previously mentioned, our photo-acoustic signal was generated by absorption in ambient moisture. In order to correlate our experiment and theory, the temperature and relative humidity in the laboratory were recorded as the photo-acoustic signal data was taken. This atmospheric information was related to the partial pressure of water vapor, and subsequently converted to the amount of water vapor present in the air in parts per million. Finally, this information was used in conjunction with HITRAN [18] in order to obtain an accurate absorption coefficient for the transition used and under the conditions at the time of the experiment. For reference, we show in Fig. 10 the water concentration as a function of temperature for various levels of relative humidity.

4 Measurement

Based on the predictions of the modeling (described in Sect. 5) a set of five cells were constructed. These cells used 2.08-mm inner diameter brass tubing with a length of nominally 35 mm. Tubing lengths varied over 34.82–35.45 mm. EK3133 microphones were located at the center, and offsets of 8.3, 10.3, 12.5, and 14.8 mm. Pictures of two cells are shown in Fig. 11a and b.

Measurements of the five cells are shown in Fig. 12. The Qs of these responses range from 3.5 for the centered mic (Fig. 11a) to 14.4 for the mic closest to the resonator end (Fig. 11b). The peak response occurs for the mic with 10.3 mm of offset and a Q of 6. Note that as the mic is offset the resonant frequency and the Q should increase. The data in Fig. 12 conforms to this generally but has some small deviations because the lengths of the tubes varied by ±1%.

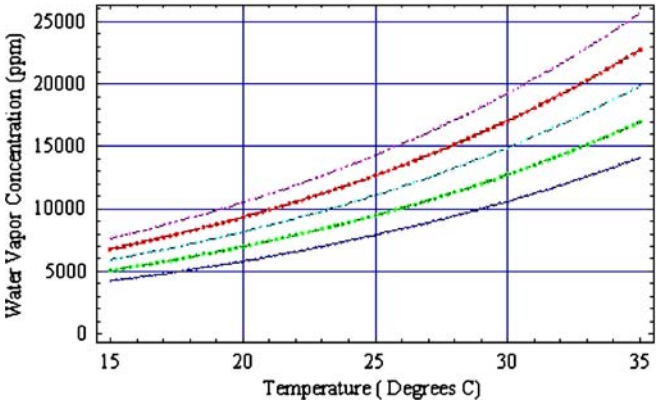

FIGURE 10 The amount of water vapor present in parts per million as a function of temperature. The relative humidity of each curve is labeled on the *right-hand side* of the curve and ranges from 25% to 45%

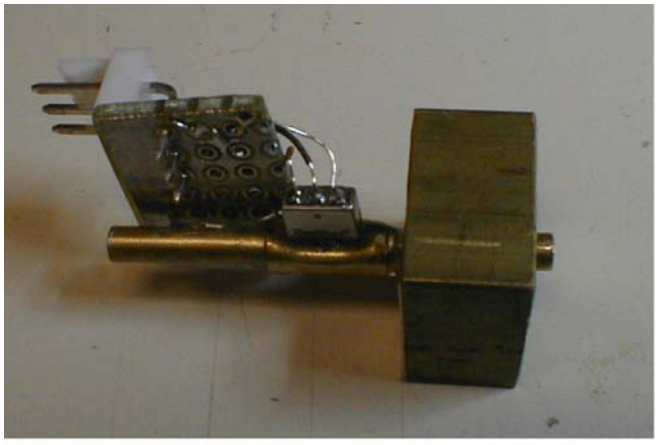

a

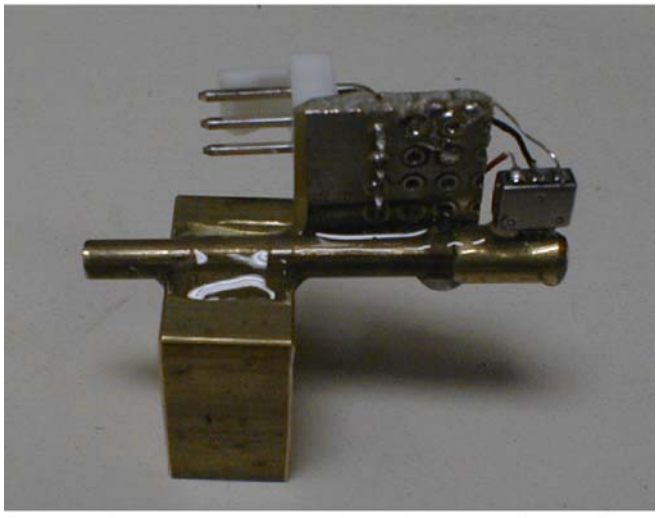

b

FIGURE 11 PAS cells used for offset microphone experiments. (**a**) centered, (**b**) offset

5 Modeling

The simple tubular cells can be modeled in many ways. One method is to use electrical equivalent circuits of the light source and acoustic elements [10, 19]. Modeling the cells shown in Fig. 11 requires electrical equivalents for the microphone acoustic impedance, the tube, the open ends of the tube, and the laser excitation. The full acoustical model from Knowles can be simplified to the loading model shown in Fig. 13. This model is dominated by the approximately 2-mm diameter by 2-mm long 'snout' that interfaces the microphone diaphragm to the outside world. This 'snout' has resistance and inductance while the back-volume determines the capacitance shown in Fig. 13.

The tube impedance can be calculated by using a transmission line with an acoustic impedance given by (3) [10, 19]. The losses of this transmission line will be dominated by boundary layer losses in this application [10]. These losses are very similar to skin effect losses in electrical circuits. This loss term is $3.09 \times 10^{-4}\sqrt{f}/r$ dB per meter, where f is the frequency in hertz and r is the radius in meters [10, 18]. This term is slightly higher than the $2.7 \times 10^{-4}\sqrt{f}/r$ developed

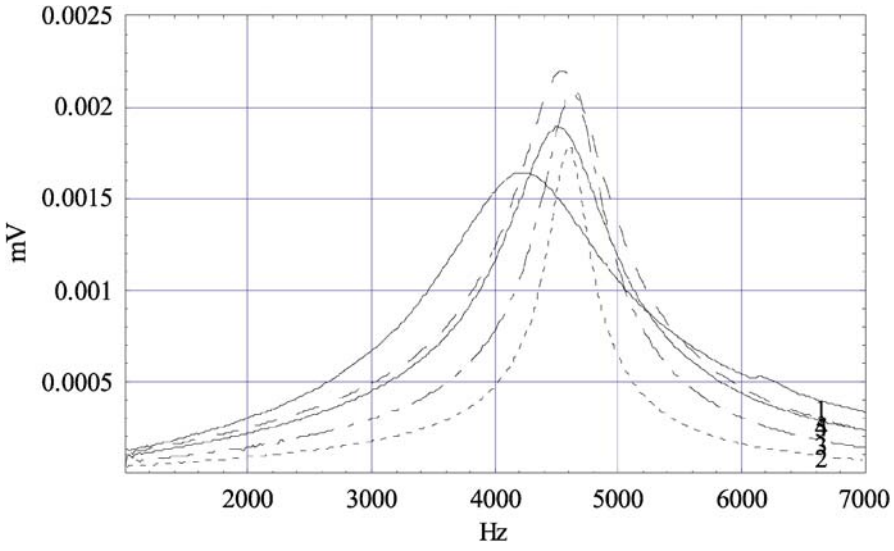

FIGURE 12 Measurements of the five cells. The *y*-axis is in mV and the *x*-axis is in hertz. The curves are numbered in the *lower right hand corner* with 1 corresponding to centered mic and 2 having the largest offset. Curves 3–5 are intermediate offsets of 12.5, 10.3, and 8.3 mm, respectively

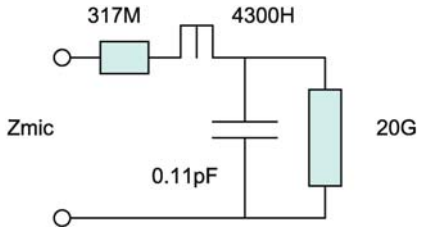

FIGURE 13 Simplified EK3133 model for acoustic loading. The *rectangles* are resistors with units of 317 MΩ (317 M) and 20 GΩ (20 G)

in most theories because it includes a correction factor for our measurements. Note that electrical simulators assume that propagation is at the speed of light and not at the speed of sound, so that the lengths in meters at a given frequency are much longer. Scaling the loss by the speed of sound divided by the speed of light ($c_{\text{sound}}/c_{\text{light}}$) will give the correct loss at the acoustic frequency. The open ends of the tube create a discontinuity at the interface to open air. This discontinuity can be modeled as a reactive term, which appears to extend the length of the tube, and a resistive term representing radiation loss [10, 19, 20]. The electrical model uses an impedance, Z_{end}, in parallel with the end of the tube transmission line. Equation (6) describes Z_{end}, with θ and χ being functions defined in Morse and Ingard [10]. Note that while the derivation in Morse and Ingard assumes an infinite flange we have a simple tube and this contributes a small error to our modeling. Also note that Morse and Ingard used a $-$i reactive term while we use a $+$j reactive term because physics and engineering have different conventions. j in (6) is taken to be the square root of -1 and all the other terms have been defined previously.

$$Z_{\text{end}} = \frac{\varrho c\,(\theta + \mathrm{j}\chi)}{\pi r^2}\,. \tag{6}$$

The final term in the model is the heating due to the laser source. This term can be modeled as a current source per unit length along the transmission line equivalent of the tube. An electrical current is analogous to an acoustic velocity and the molecular heating creates motion. The strength of the current source is given in (7) as a combination of the laser power, molecular absorption, modulation method, and relative humidity.

$$I_{\text{T}} = \frac{m\,(\gamma - 1)\,P\alpha l}{\varrho c^2}\,. \tag{7}$$

In (7), I_{T} is the total equivalent current, m is the modulation method factor for $2f$ operation, 0.34/1.414, P is the laser power, α is the absorption in inverse cm, and l is the length in cm. For 10 000-ppm moisture α equals 0.014. Previous analysis has included everything but the modulation method [11]. The modulation method is particularly important because we are measuring the alternating component of the pressure with the microphone. In Sect. 3 the $2f$ modulation method was shown to give a factor of 0.34 conversion from average optical power to peak variation. We also need to divide this by 1.414 to convert peak to root mean square variations. Our electrical equivalent cell model is shown in Fig. 14. This model is made of many transmission line segments which are short compared to a wavelength. These segments make it easier to introduce the distributed current source required by the optical heating.

As a final step we take the pressure at the microphone and convert it to voltage out of the microphone. The EK3133s have a very flat transfer function with about 17 mV/Pa conversion efficiency in our frequency range.

5.1 *Additional modeling*

The system was also modeled using a formalism developed by Bernegger and Sigrist [21]. Their formalism at root also uses an analogy between acoustical and electrical systems. However, the model uses a system-oriented approach by which the pressure and volume velocity of each segment of tubing are described by a transfer matrix, T, and a vector, $\boldsymbol{w}$. The matrix T accounts for propagation of the sound wave through the tube, while the vector $\boldsymbol{w}$ describes the outgoing sound wave generated in the tube by absorption of optical radiation.

The photo-acoustic resonator is generalized to a one-dimensional cell and divided into a finite number of sections, each characterized by its length, circumference, and cross-sectional area. The propagation from an initial point

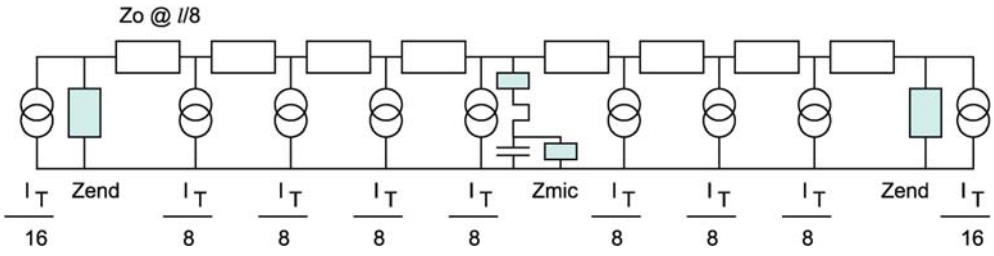

FIGURE 14 Equivalent electrical analog for the PAS cell with a centered microphone

(typically an end point) is then modeled by matrix multiplication. Each change in tube diameter or any ports on the cell are accounted for by their own matrices. Ports off the main resonator which are not illuminated are characterized by transfer matrices, but will not have a vector $\boldsymbol{w}$ associated with them as they do not absorb optical power. When a full transfer matrix from end to end of the cell is developed, the system of equations is solved simultaneously with the addition of another set of equations. This set of equations is provided by boundary conditions at the end of the tube. In our system here, the acoustic radiation impedance of the tube ends has been approximated using the well-known solution of acoustic radiation from a piston [10, 20]. The addition of these boundary equations allows the solution of the equations for the pressure and volume velocity at one end of the cavity. Again utilizing the transfer matrices, this initial pressure and volume velocity is transformed to the pressure and volume velocity at the point of interest in the cavity.

6 Comparison of results and models

Using this formalism and a simplified model for the Knowles electret, we have also solved for the signal level in the cavity as a function of the microphone position. Shown below in Fig. 15 is the comparison of the experiment and theory with the microphone mounted at a point approximately 12 mm off center. The formalism of [21] was used for this modeling. The slight shift in the peak of the curves is likely due to differences between the microphone model and the actual microphone. Slight imperfections and/or manufacturing tolerances in individual microphones can easily account for variations in the response. Specifically, the microphone diaphragm, as well as the length and diameter of the chamber leading to the diaphragm, will all change the impedance of the microphone. These deviations in impedance will lead to differences in the amplitude and frequency of the acoustic resonance.

We can also compare the cell responses versus offset position. Figure 16 shows the response in millivolts of the measured cell (solid line), the predicted response (dashed line), and a cell with an ideal microphone of infinite impedance (alternating line). Note that the cell with an infinite-impedance microphone approximates half a cosine and has its millivolts divided by 5 (it has five times the response shown). Several interesting facts are shown in Fig. 16. First, the microphone loading can substantially reduce the signal at the center of the cell. Second, moving the microphone off center can actually increase the signal at the microphone. Third, the signal does not go to zero at the physical end of the cell because of Z_{end}, the radiation impedance at the end of the tube. Fourth, we can see that the simulated peak voltage is around 13.5 mm offset while the measured peak is closer to 11 mm offset. This means that the microphone impedance is larger than that given in the model because the offset for maximum response is inversely proportional to the microphone resistance.

Another result of moving the microphone off center of the cavity in microphone-dominated cells is that the Q of the cell will increase as the microphone is moved off center, as shown

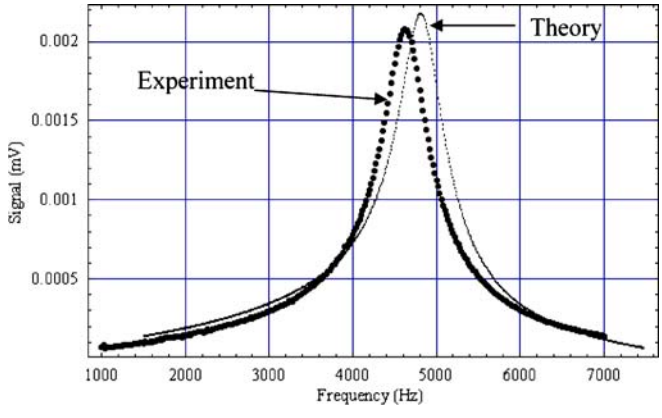

FIGURE 15 Comparison of the transfer matrix model (including microphone loading) to the experimental data using the model in [21]. The microphone is approximately 12 mm off center in the cavity. The *heavy dots* are the experiment and the *light dots* are the theory

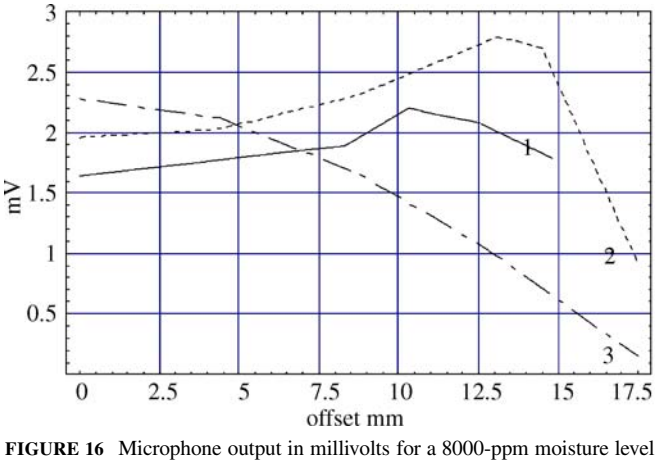

FIGURE 16 Microphone output in millivolts for a 8000-ppm moisture level as the microphone is moved from the center of the cell to the end of the cell. The y-axis is in millivolts and the x-axis is in mm. The *solid line* (1) is the measured data, the *dashed line* (2) is the simulated data, and the *alternating line* (3) is for a cell with a microphone of infinite impedance and is scaled by 1/5

in Fig. 12. The physical reasoning behind this is that when the microphone is at the center of the cavity the microphone dominates the Q, and as the microphone is offset the cell Q increases to that of the cavity alone.

7 Conclusions

We have presented theory and experiments showing the importance of microphone loading in small-diameter photo-acoustic cells. Our theory includes factors such as the cell physical parameters, laser power, molecular absorption, $2f$ modulation efficiency, and microphone transfer function. Including all of these factors allows us to present simulation results in millivolts out of the microphone for a given laser power input.

Our results show that seemingly counter-intuitive microphone placements away from the center of a resonant tube can result in increased microphone signal outputs. While ideally microphones would be chosen of sufficiently high impedance to not load the cell, practical microphones have a finite acoustic impedance which can be substantially lower than the resonant impedance of a small cell. Optimizing a small cell for maximum sensitivity is not just a matter of designing a cell with a large pressure to laser power ratio (Pa/W) and choosing a microphone with a high sensitivity (mV/Pa), but also includes accounting for the microphone interaction with the acoustic cell.

REFERENCES

1 A.G. Bell, Am. J. Sci. **20**, 305 (1880)
2 A.G. Bell, Philos. Mag. **11**, 510 (1881)
3 L.B. Kreuzer, J. Appl. Phys. **42**, 2934 (1971)
4 Y.-H. Pao (ed.), *Optoacoustic Spectroscopy and Detection* (Academic, New York, 1977)
5 M. Szakall, Z. Bozoki, A. Mohacsi, A. Varga, G. Szabo, Appl. Spectrosc. **58**, 792 (2004)
6 J.P. Besson, S. Schilt, L. Thevanaz, Spectrochim. Acta A **60**, 3449 (2004)
7 A. Miklos, P. Hess, Z. Bozoki, Rev. Sci. Instrum. **72**, 1937 (2001)
8 S. Firebaugh, J. Microelectromech. Syst. **10**, 232 (2001)
9 S. Firebaugh, *Miniaturization and Integration of Photoacoustic Detection*, Ph.D. thesis, MIT (2001)
10 P.M. Morse, K.U. Ingard, *Theoretical Acoustics* (Princeton University Press, Princeton, 1968)
11 S. Bernegger, M.W. Sigrist, Appl. Phys. B **44**, 125 (1987)
12 T.H. Lee, *Planar Microwave Engineering* (Cambridge University Press, Cambridge, 2004)
13 S. Schilte, L. Thevanaz, P. Robert, Opt. Lett. **42**, 6728 (2003)
14 C. Edwards, G. Barwood, P. Gill, B. Schirmer, H. Venzke, A. Melling, Appl. Opt. **38**, 4699 (1999)
15 A. Siegman, *Lasers* (University Science Books, Mill Valley, CA, 1986)
16 P. Kluczynsky, O. Axener, Appl. Opt. **38**, 5803 (1999)
17 J. Reid, D. Labrie, Appl. Phys. B **26**, 203 (1981)
18 www.hitran.com
19 L.E. Kinsler, A.R. Frey, *Fundamentals of Acoustics* (Wiley, New York, 1962)
20 H. Levine, J. Schwinger, Phys. Rev. **73**, 383 (1948)
21 S. Bernegger, M.W. Sigrist, Infrared Phys. **30**, 375 (1990)
22 A. Riddle, Patent application (USA, June 2005)
23 F.G.C. Bijnen, J. Reuss, F.J.M. Harren, Rev. Sci. Instrum. **67**, 2914 (1996)